Journal of Chromatography A, 1218 (2011) 3781–3790

Contents lists available at ScienceDirect

Journal of Chromatography A

journal homepage: www.elsevier.com/locate/chroma

Surface modification of high-performance polymeric fibers by an oxygen plasma. A comparative study of poly(*p*-phenylene terephthalamide) and poly(*p*-phenylene benzobisoxazole)

K. Tamargo-Martínez*, A. Martínez-Alonso, S. Villar-Rodil, J.I. Paredes, M.A. Montes-Morán, J.M.D. Tascón

Instituto Nacional del Carbón, INCAR-CSIC, Apartado 73, 33080 Oviedo, Spain

ARTICLE INFO

Article history:
Received 18 January 2011
Received in revised form 11 April 2011
Accepted 11 April 2011
Available online 29 April 2011

Keywords:
Oxygen plasma treatment
Surface modification
High-performance fibers
Inverse gas chromatography (IGC)
Atomic force microscopy (AFM)

ABSTRACT

Poly(*p*-phenylene terephthalamide) (PPTA) and poly(*p*-phenylene benzobisoxazole) (PBO) fibers were exposed to an oxygen plasma under equivalent conditions. The resulting changes in the surface properties of PPTA and PBO were comparatively investigated using inverse gas chromatography (IGC) and atomic force microscopy (AFM). Both non-polar (*n*-alkanes) and polar probes of different acid–base characteristics were used in IGC adsorption experiments. Following plasma exposure, size-exclusion phenomena, probably associated to the formation of pores (nanoroughness), were detected with the largest *n*-alkanes (C_9 and C_{10}). From the adsorption of polar probes, an increase in the number or strength of the acidic and basic sites present at the fiber surfaces following plasma treatment was detected. The effects of the oxygen plasma treatments were similar for PPTA and PBO. In both cases, oxygen plasma introduces polar groups onto the surfaces, involving an increase in the degree of surface nanoroughness. AFM measurements evidenced substantial changes in the surface morphology at the nanometer scale, especially after plasma exposure for a long time. For the PBO fibers, the outermost layer – contaminant substances – was removed thanks to the plasma treatment, which indicates that this agent had a surface cleaning effect.

1. Introduction

Poly(*p*-phenylene benzobisoxazole) (PBO) has deserved considerable attention in both basic and applied areas of research on high-performance materials [1–8]. PBO belongs to the new class of high-performance rigid-rod materials. The repeat chemical structure is as follows:

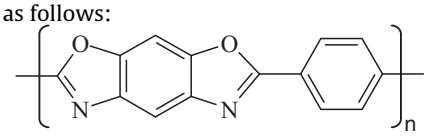

This chemical structure confers to PBO an excellent thermal stability [9], chemical resistance and specific stiffness and strength [10]. Therefore, PBO provides great potential applications such as reinforcing fibers for composites (FRC). Nevertheless, PBO fiber-reinforced composites generally show a poor interfacial adhesion between untreated fibers and matrix resin [11], due to the inert nature of the PBO fiber. In consequence, as the load transfer through the interface is related to the interfacial interactions, it is necessary to improve the interfacial bonding or adhesion by increasing either the number of interactions or the bond strength. In this sense, several surface modification methods have been proposed for some polymeric fiber materials, including chemical (electrolytic oxidation, coupling agents) [12,13,15–20], or plasma treatments [14,21]. One peculiar advantage of the low-pressure plasma treatment is that it can be used to modify the chemical and physical states of a surface without altering the bulk fiber properties [22].

Therefore, the knowledge of the fiber surface energetics is essential for the specific design of interfaces since the adhesion is determined by chemical and physical structures of both, fiber and matrix. Inverse gas chromatography (IGC) at infinite dilution is a straightforward and very sensitive technique for the thermodynamic characterization of polymer surfaces [23] since it is versatile, robust, user-friendly and inexpensive. In a previous work, a number of differently solvent-scoured commercial PBO fiber samples have been studied using IGC [24] in order to establish the efficiency of the different cleaning solvents and determine the thermodynamic properties of the pristine PBO surface.

In this work, the effects of oxygen plasma treatment on the surface characteristics of PBO fibers were investigated through the study of their interaction with both non-polar and polar probe molecules using IGC. For comparison, samples of oxygen plasma-

* Corresponding author. Tel.: +34 985119090; fax: +34 985297662.
E-mail address: katia@incar.csic.es (K. Tamargo-Martínez).

0021-9673/$ – see front matter © 2011 Elsevier B.V. All rights reserved.
doi:10.1016/j.chroma.2011.04.028

Table 1
Sample codes.

Plasma treatment conditions			Fibers	
Power	Gas	Time	PPTA	PBO
70 W	O_2	1 min	KO 1	ZO 1
		4 min	KO 4	ZO 4

treated poly(*p*-phenylene terephthalamide) (PPTA) fibers were prepared and characterized under identical experimental conditions. The results obtained with PPTA are taken as a reference since some previous knowledge is available on the surface thermodynamics of this material [25]. As a complementary technique, atomic force microscopy (AFM) was employed to monitor the changes in surface structure induced by the oxygen plasma treatments on both polymeric fibers. The objective was to determine whether there is a relationship between topographic properties of the fiber surfaces and the thermodynamic magnitudes determined by IGC.

2. Experimental

2.1. Materials

Two types of polymeric fibers have been used as starting materials for this work.

PPTA: Finish-free Kevlar®-29 fibers – supplied by E.I. DuPont de Nemours, which were used as received (referred as sample K). The yarn is made of 1000 filaments of ~12.1 μm diameter and the specific linear density is 964 dtex.

PBO: Zylon® HM fiber yarn – supplied by Toyobo (referred as sample Z). The manufacturer filament diameter was ~11.2 μm and the specific linear density of the yarns was 545 dtex.

For PPTA and PBO fibers, the average molecular weight is very similar each other. It is of the order of 20,000–40,000 depending on the processing parameters which are unknown in our case.

Plasma treatments were carried out in a plasma processor, Technics Plasma 200-G. An oxygen (99.9990% pure) gas flow was introduced so as to maintain a pressure of 1.0 mbar inside the reaction chamber. Fresh PPTA and PBO were treated at 70 W of microwave (2.45 GHz) plasma power, during one or 4 min, respectively. Reference codes for the plasma-treated samples are given in Table 1.

2.2. Methods

2.2.1. Thermodynamic parameters and adsorption measurements

The fundamental parameter measured by IGC is the net retention volume V_N defined as the volume of carrier gas required to elute a given zone of solute vapor [26]. This parameter is estimated, for a given probe, from the measured retention time, t_R:

$$V_N = (t_R - t_m) \cdot F \tag{1}$$

where F is the flow rate and t_m is the gas hold-up time.

V_N is directly related to the partition coefficient for the solute surface K_s [27] according to Eq. (2):

$$V_N = K_s A \tag{2}$$

where A is the total surface area of the stationary phase. If the adsorption experiments are carried out under very low adsorbate concentration, i.e., in the limit of infinite dilution, the interactions between adsorbate molecules are negligible and the adsorption is described by Henry's law and K_s is then directly proportional to the Henry's constant [27]. The previous equation is valid as long as the bulk absorption of the probe in the stationary phase is negligible [26]. Thermodynamic functions of the adsorption process at infinite dilution can be thus calculated from K_s [28]:

$$\Delta G_a^0 = RT \ln V_N = RT \ln \left(K_s \frac{p_{s,g}}{\pi_s} \right) \tag{3}$$

$$q_d^0 = \left[\frac{\partial(\Delta G_a^0/T)}{\partial(1/T)} \right]_p = \left[\frac{\partial(\ln\ K_s)}{\partial(1/T)} \right]_p \tag{4}$$

where $p_{s,g}$ is a reference pressure having a value of 1 atm (101 kN m^{-2}) and π_s is the two-dimensional pressure of the adsorbed state, 0.338 mN m^{-1} [29]. From the adsorption standard free energies and standard enthalpies, adsorption entropies can be calculated straightforwardly according to Eq. (5):

$$-\Delta S_a^0 = \frac{q_d^0 - \Delta G_a^0}{T} \tag{5}$$

Selection of the probes to be used in IGC studies of solid surfaces depends on the type of information that should be gathered. In the case of high performance fibers, it is interesting to determine parameters related to their surface microstructure, such as textural and energetic parameters. Also, information related to their surface chemistry, i.e., acid–base properties is of key relevance.

For the first purpose, there is a well-established experimental procedure consisting of the elution of linear *n*-alkanes through the stationary phase. According to the early concepts of Riddle and Fowkes on the nature of the interaction at interfaces, *n*-alkanes are only capable of dispersive interactions [30]. Based on this, Dorris and Gray [31] proposed a calculation method in which the difference in the free energy of adsorption of two *n*-alkanes with succeeding values of $n(-\Delta G_a^{CH_2})$ was used to calculate the dispersive component of the surface free energy of the stationary phase, γ_s^D:

$$\gamma_s^D = \frac{1}{4N_A^2 a_{CH_2}^2} \frac{(-\Delta G_a^{CH_2})^2}{\gamma CH_2} \tag{6}$$

where N_A is Avogadro number, a_{CH_2} is the area of a methylene group (0.06 nm^2) [31], and γ_{CH_2} is the surface tension of ideal liquid polyethylene; the latter parameter is computed as a function of temperature as follows:

$$\gamma_{CH_2}[\text{mJ/m}^2] = 35.600 - 0.058[T(^\circ\text{C}) - 20] \tag{7}$$

where T is the temperature in °C.

On the other hand, if polar probes are injected into the column instead of *n*-alkanes, the adsorption of the adsorbate molecules on the stationary phase involves not only dispersive but also specific interactions [32–35]. Thus, $-\Delta G_a^0$ is assumed to be the sum of two independent contributions accounting for both types of molecular interaction:

$$\Delta G_a^0 = \Delta G_a^D + \Delta G_a^p \tag{8}$$

The additional contribution $-\Delta G_a^p$ can be estimated in different ways by the elution of polar probes (at infinite dilution conditions) covering a wide range of acid–base character. The method proposed by Donnet et al. [36], which takes into account the molecular polarizability of the different adsorbates, seems to be particularly reliable with regard to the specific (acid–base) interactions on relatively high energetic surfaces. According to such method, the dispersive component of the free energy of interaction of any probe with a surface at infinite dilution conditions can be, at a first approximation, estimated from a simplified version of the London equation:

$$-\Delta G_a^0 = K(h\nu_S)^{1/2}\alpha_s \cdot (h\nu_L)^{1/2}\alpha_L + C \tag{9}$$

where K and C are constants, h is the Planck's constant, ν_S and ν_L are characteristic electronic frequencies corresponding to solid (S)

and probe (L), and α_s and α_L are the deformation polarizabilities. In the case of the *n*-alkanes adsorption ($-\Delta G_a^p = 0$), a plot of $-\Delta G_a^0$ *vs* $[(h\nu_L)^{1/2}\cdot\alpha_L]$ should render a straight line. As "$K(h\nu_s)^{1/2}\cdot\alpha_s$" term is characteristic of a given solid surface [36], $-\Delta G_a^p$ of the different polar probes is finally obtained, at a given temperature, from differences between their $-\Delta G_a^0$ calculated from Eq. (3) and the reference line composed with data obtained from the elution of the linear *n*-alkanes.

Adsorption measurements were carried out by IGC under infinite dilution conditions using a Hewlett-Packard 5890-II gas chromatograph equipped with a high sensitivity (10^{-12} mol) flame ionization detector. Continuous fiber yarns (~1.0 g) were packed into approximately 480 mm long passivated nickel columns (2.4 mm i.d.). Before each series of experiments, the chromatographic columns were preconditioned by heating at 383 K under a constant helium flow. Typical conditioning times of 12 h were necessary to achieve reproducible results. Once conditioned, the helium flow was kept through the columns in the course of the adsorption experiments in order to prevent any sample contamination.

Adsorption experiments were carried out at 10 K intervals in the 303–343 K temperature range. Small amounts (0.1–1.0 μl) of selected probe compounds-measured with a 10 μl Hamilton syringe were eluted through the columns. *n*-Alkane vapors (C_7–C_{12}, >99% pure) were injected at infinite dilution conditions (see above) to establish the γ_s^D of the different fiber surfaces, whereas changes in the surface chemistry were evaluated by injecting benzene, nitromethane, acetonitrile, pyridine, acetone, *t*-butyl alcohol, ethyl acetate and tetrahydrofuran (all of them >99.0% pure). Al least, five injections of each alkane were carried out at each temperature and methane was injected simultaneously to determine dead volumes in the column. Helium (99.9995% pure) was used as carrier gas, with typical flow rates *F* of ~20 ml min^{-1}. This value was set after correcting the flow rate measured at the column outlet with a bubble flow meter (F_f):

$$F = jF_f \frac{T}{T_f}\left[\frac{P_{out} - P_w}{P_{out}}\right] \quad (10)$$

$$j = \frac{3}{2}\left[\frac{(P_{in} - P_{out})^2 - 1}{(P_{in} - P_{out})^3 - 1}\right] \quad (11)$$

where T and T_f are the temperatures of the column and flowmeter, respectively, P_w is the water vapor pressure of the bubble and P_{out} and P_{in} are the pressures at the outlet and inlet, respectively [26].

2.2.2. AFM imaging

AFM measurements were carried out in a Nanoscope Multimode IIIa apparatus, from Veeco, in air, at room temperature and using the tapping mode of operation. Rectangular silicon cantilevers (Veeco) with spring constants between 20 and 100 N m^{-1} and nominal tip radii of curvature of 5–10 nm – as specified by the manufacturer – were employed. Their typical resonance frequencies were around 250 kHz. Sparse bundles of starting and plasma-treated PPTA and PBO fibers were mounted onto metallic sample holders using a double-sided carbon adhesive tape. Special care was required to avoid the presence of fibers sticking out from the sample surface, since they could touch the cantilever at points other than the very tip apex and invalidate the measurement. To ensure that the features detected in the images were representative of the analyzed samples, many different fibers were investigated and many different areas on each fiber were surveyed.

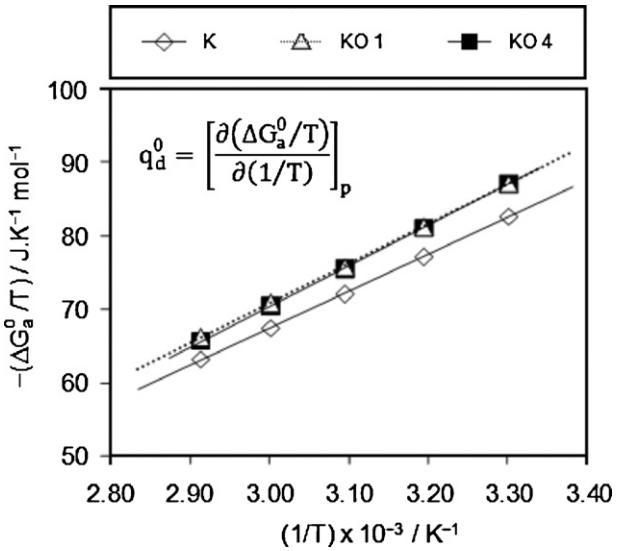

Fig. 1. Variation of $(-\Delta G_a^0/T)$ with (1/T) for the adsorption of *n*-nonane on the PPTA fibers under study. The slope of curves represents the differential heat of *n*-nonane onto the PPTA fibers surfaces.

3. Results

3.1. Adsorption of n-alkanes at infinite dilution conditions

In the case of *n*-alkanes, the chromatographic peaks obtained were mainly symmetrical, and the location of their maxima did not depend on the amount of probe injected. This ensured that the adsorption was taking place in the linear part of the isotherm (Henry's law). Thus the retention times of the *n*-alkanes were measured at the peak maximum. Methane was used to correct the dead time t_m (Eq. (1)) in the column so that it was injected at the same time that each molecular probe. V_N of the *n*-alkanes did not change with the flow rate, thus indicating that the adsorption equilibrium was attained. Fig. 1 illustrates the linear dependence of $(-\Delta G_a^0/T)$ as a function of $(1/T)$ obtained for *n*-nonane adsorption on the various studied PPTA samples. This behavior, which is extensive to the rest of the *n*-alkane-PPTA and *n*-alkane-PBO systems, indicates that q_d^0 is constant within the considered temperature range.

Table 2 shows the values of the differential heats of adsorption at zero coverage for the linear *n*-alkanes on the fiber samples. The standard deviations in q_d^0 data were never >2.0%. The values obtained for the PPTA fibers were very similar to those published previously [25,37]. Sample KO 1 reveals the highest differential heats of adsorption for all the tested hydrocarbons. In the case of PBO, the values for q_d^0 corresponding to the plasma-modified samples are greater in absolute value than the one for the starting material, Z; the most exothermal ones corresponding to ZO 4 sample.

In all cases (plasma-treated PPTA and PBO samples) it was checked that, for each *n*-alkane, it fulfilled that $q_d^0 \geq -\Delta H_{liq}^a$. The behavior exhibited by the plasma-treated PPTA samples as well as ZO 4 ($q_d^0 > -\Delta H_{liq}^a$) is typical of adsorption processes where the adsorbate–adsorbent interactions are stronger than the adsorbate–adsorbate ones, and this typically occurs in high-crystalline polymers [38]. High q_d^0 values are produced when the adsorption process takes place in micropores with a size close to the molecular dimension of the probe, so that the closer the molecular dimension and the pore width, the higher the enthalpy [39,40]. In the case of ZO 1, q_d^0 values are very close to $-\Delta H_{liq}^a$ data (Table 2). This could mean that the adsorption process takes place in the external surface [40].

Table 2
Differential heats of adsorption of *n*-alkanes, q_d^0(kJ mol^{-1}), and standard liquefaction enthalpies at 323 K – ΔH_{liq}^a (kJ mol^{-1}).

n-Alkanes	K	KO 1	KO 4	Z [24]	ZO 1	ZO 4	Z washed with ethanol [24]	$-\Delta H_{liq}^a$
C_7		43.2	43.2			40.5	45.0	35.0
C_8	45.9	49.8	48.3	34.9	39.3	43.2	51.5	39.8
C_9	50.8	55.9	54.5	38.0	45.0	48.6	58.1	44.6
C_{10}	55.8	61.6	60.5	42.0	49.7	55.1	65.3	49.4
C_{11}	60.1	64.9	63.6	45.9	54.6	59.1	69.6	54.2
C_{12}				49.5	55.6			58.9

Table 3
Standard entropies of adsorption of *n*-alkanes, experimental, $-\Delta S_a^0$(J K^{-1} mol^{-1}), and calculated according to de Boer's model at 303 K – ΔS_{th}^0 (J K^{-1} mol^{-1}).

n-Alkanes	K	KO 1	KO 4	Z [24]	ZO 1	ZO 4	Z washed with ethanol [24]	$-\Delta S_{th}^0$
C_7		76.7	76.0			73.2	77.4	52.6
C_8	79.2	87.7	82.6	47.9	66.9	72.8	87.1	53.2
C_9	85.1	97.6	92.9	50.0	77.0	81.2	97.2	53.6
C_{10}	91.8	106.1	102.6	55.1	83.5	92.9	108.7	54.0
C_{11}	95.8	107.0	103.0	59.8	90.8	96.8	111.6	54.4
C_{12}				64.0	86.6			54.8

Table 4
Values of γ_s^D(mJ m^{-2}) at different temperatures.

T (K)	K	KO 1	KO 4	Z [24]	ZO 1	ZO 4	Z washed with ethanol [24]
343	43.8	45.9	44.3	28.9	33.6	38.6	60.4
333	47.6	47.3	46.2	29.7	33.8	40.4	63.8
323	50.9	49.5	48.3	30.7	35.9	42.7	65.3
313	52.5	56.6	50.9	32.1	36.5	44.6	66.6
303	54.0	55.1	53.0	32.7	39.1	48.5	69.4
293[a]	57.3	57.1	55.1	33.8	40.4	50.2	71.3

[a] Obtained by extrapolation.

On the other hand, it is observed that the standard differential heat of adsorption decreases slightly while the plasma exposure time of PPTA increases. The opposite trend is observed in the case of PBO (Table 2). The analysis of the adsorption heat results (Table 2) reveals that the process is more exothermal with PPTA samples than with the PBO ones.

The $-\Delta S_a^0$ results listed in Table 3 are the average data calculated according to Eq. (5) at different temperatures. The last column in this table gives the values predicted by de Boer's model ($-\Delta S_{th}^0$). In all cases, the obtained $-\Delta S_a^0$ data were independent of temperature. As Table 3 shows, the experimental adsorption entropies are in most cases greater (in absolute value) than those predicted by the bidimensional gas model, what implies that the surface is more ordered than as expected by de Boer's model. This means, at the same time, that the adsorbed hydrocarbons have lost some vibrational and/or rotational degrees of freedom.

Systematic differences have been found between the thermodynamic magnitudes of adsorption (Tables 2 and 3) measured on the plasma-modified fibers for the largest *n*-alkanes (C_8 and C_9 for KO 1 and KO 4, and C_9 and C_{10}, for ZO 1 and ZO 4) and the rest of the hydrocarbons. A similar trend has been observed for plasma-treated PPTA fibers [25] and also for washed PBO fibers [24]. The behavior described for the largest alkanes was justified as a result of a size-exclusion behavior, either because (i) the nanopore sizes are close to the probe molecular dimensions (largest alkanes) or (ii), in infinite dilution conditions (in which the IGC processes occur) the molecules are adsorbed onto the most energetic sites [24,25]. Table 4 lists the values of γ_s^D at several temperatures, obtained from Eq. (6). In all cases, linear expressions [γ_s^D *vs T* (°C)] fitted reasonably well the experimental data. Values of γ_s^D at 293 K were subsequently calculated by extrapolation, and they are included in the last row of Table 4. For K sample, the extrapolated γ_s^D value is 57.3 mJ m^{-2}, being relatively high and typical of a polymer with a high crystallinity degree [25,37].

Following the 1-min plasma treatment, the γ_s^D values for KO 1 were practically equivalent to those measured for the starting material, K; however, for sample KO 4, they decreased by about 1.5 mJ m^{-2}. Similar small differences in γ_s^D brought about by plasma treatment have been reported in previous works [25,41].

For the Z surface, the extrapolated γ_s^D value at 293 K was 33.8 mJ m^{-2}. This value is relatively low for a highly crystalline polymeric fiber, especially as compared to K sample, which is less crystalline than PBO fiber [42,43]. It has been demonstrated that the presence of a small amount of contaminant substances on polymeric fiber surfaces – specifically on PBO – strongly decreases the dispersive component of the surface tension [24]. The oxygen plasma treatments produce increases in γ_s^D of 6 (1 min) and 16 mJ m^{-2} (4 min) (Table 4). For the plasma-treated PBO fibers, the dispersive component of the free surface energy follows the same trend as for the other thermodynamic magnitudes (q_d^0 and $-\Delta S_a^0$) with the plasma treatments (Tables 2–4). In particular, the q_d^0, $-\Delta S_a^0$ and γ_s^D values obtained for ZO 4 are typical of highly crystalline polymers. A similar trend (see Tables 2–4) was reported for high-modulus PBO fibers subjected to extraction with ethanol in order to remove their surface contaminants [24]. This suggests that the 4-min plasma treatment has produced some surface cleaning.

3.2. Adsorption of polar probes at zero coverage

The ability of polar probes to donate or accept electrons has been parameterized by means of the donor number (DN) and acceptor number (AN*), respectively [44]. Table 5 lists the (DN) and (AN*) parameters for the probes used in this work [30,45,46].

Slight concentration-dependent effects were observed for the elution of polar probes through all the chromatographic columns due to the so-called "slow kinetic processes" [26]. This behavior is indicative of surface heterogeneity, whereby some of the different active sites contained onto the surface interact strongly with the

Table 5
Donor numbers (DN) and acceptor numbers (AN*) of the polar probes used in this work.

Polar probes	Character	DN (kJ mol^{-1})	AN* (kJ mol^{-1})
Benzene	Apolar	0.42 [45]	0.71 [45]
Nitromethane	Acid*	11.29 [45]	17.97 [45]
Acetonitrile	Amphoteric	58.94 [45]	19.65 [45]
Pyridine	Basic*	138.36 [45]	0.59 [45]
Acetone	Amphoteric	71.06 [45]	10.45 [45]
t-Butyl alcohol	Acid**	91.54 [46]	31.77 [30]
Ethyl acetate	Amphoteric	71.48 [45]	6.27 [45]
Tetrahydrofuran	Basic*	83.60 [45]	2.09 [45]

* Medium.
** Strong.

probes slowing their desorption [25,45,47]. To reduce the degree of peak asymmetry, it was necessary to work at extremely low probe concentrations. Retention times were estimated from the first momentum of peaks obtained at such conditions. Thus, similar thermodynamic properties to those described for the elution of *n*-alkanes were obtained for the injected polar probes.

Fig. 2 shows the variation of $-\Delta G_a^0$ *vs* $[(h\nu_L)^{1/2}\cdot\alpha_L]$ for all the polar probes on K sample at 323 K. Specific interactions $-\Delta G_a^p$ were determined, at a given temperature, from the differences between the $-\Delta G_a^0$ value for each probe capable of specific interactions and the corresponding value at the same $[(h\nu_L)^{1/2}\cdot\alpha_L]$ on the reference line composed of data obtained from the elution of *n*-Alkanes [Eq. (9)].

Table 6 shows the results obtained for the different systems under consideration. Nevertheless, for a better assessment of the obtained results, relevant $(-\Delta G_a^p)$ data are plotted in Fig. 3 for all samples of PPTA and PBO fibers under study at the specified temperatures. Moreover, from the variation of $-\Delta G_a^p$ *vs* $(1/T)$, as stated in Eq. (4), the value of the specific enthalpy of adsorption $(-\Delta H_a^p)$ was calculated for each polar probe. The corresponding values are collected in Table 7.

The values of $-\Delta G_a^p$ and $-\Delta H_a^p$ are used as parameters to compare the acid–base character of the different PPTA and PBO surfaces under study. In this work, the $-\Delta G_a^p$ data were positive for all the polar probes examined with all the tested PPTA and PBO samples – treated and untreated fibers – (see Table 6 or Fig. 3). This evidences that the polar probes establish polar interactions with all PPTA and PBO samples.

For the two starting materials (K and Z), the largest $-\Delta G_a^p$ values (Table 6) corresponded to acetonitrile (amphoteric), pyridine (moderately basic), and nitromethane (weakly acidic). They are followed by acetone (amphoteric), *t*-BuOH (acidic), ethyl acetate (amphoteric) and tetrahydrofurane (amphoteric). The values obtained for acetone and *t*-BuOH were slightly higher (~15.0%) than those for ethyl acetate and tetrahydrofurane on K sample, but were similar to each other on Z surface. Finally, the lowest values were obtained for benzene – a non-polar probe that can only establish interactions through the π electron cloud, what means that the interaction with the aromatic part is very weak.

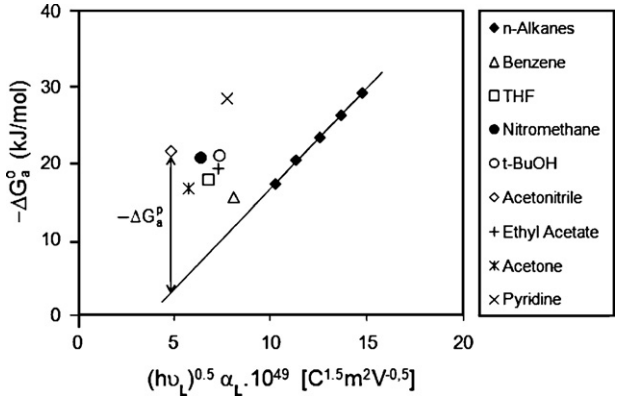

Fig. 2. Graphical description of the method followed to obtain the specific contribution of the adsorption free energy $-\Delta G_a^p$ measured for the different polar probes on K sample. The solid line corresponds to the *n*-alkanes trend line.

Nevertheless, several differences between these two magnitudes can be observed for K sample, whereas in the case of Z the $-\Delta H_a^p$ values measured for polar probes (Table 7) follow practically the same sequence as for the specific free energy of adsorption $(-\Delta G_a^p)$. The largest values of $-\Delta H_a^p$ corresponded to pyridine and *t*-BuOH. They were followed by acetonitrile and acetone; then, nitromethane and THF, and finally benzene. However, these two magnitudes have different meanings, since $-\Delta H_a^p$ does not include all the factors associated with $-\Delta G_a^p$ (Eq. (5)). In fact, $-\Delta H_a^p$ represents the chemical affinity between the adsorbate and the adsorbent, so that the specific interactions (acid–base, hydrogen bonds, etc.) are a function of the chemical characteristics (nature of the bonds, dipolar moment, acid–base properties, reaction medium, etc.) of each component (polar probe and polymeric fiber). In this sense, Rebouillat et al. [48] concluded that the PPTA surface establishes two types of specific interactions with *n*-hexylamine: acid–base and hydrogen bonds. However, $-\Delta G_a^p$ also accounts for the relative orientation of the adsorbate regarding the adsorbent. The model proposed by Hunter and Sanders [49] assumes that the attractive, or repulsive, force involved in the interaction between two idealized π systems depends on the relative orientation of their structures, which allows to establish π–π interactions to different extents.

Therefore, according to the level of interaction of the polar probes with K and Z polymeric surfaces based on $-\Delta G_a^p$ and $-\Delta H_a^p$ data, it is not simple to determine the acidic or basic nature based on the acceptor or donor number concepts [44]. A previous work [25] has indicated that the use of specific parameters such as $-\Delta G_a^p$ and $-\Delta H_a^p$ does not allow one to establish the absolute acid or basic character of the materials under consideration. On the basis of these data, it can be only stated that the PPTA and PBO surfaces contain both slightly acidic and basic sites.

Finally, it can be observed that for all the polar probes, the measured values of $-\Delta G_a^p$ and $-\Delta H_a^p$ were higher on K than on Z, with the exception of benzene (Fig. 3, Tables 6 and 7). This indicates that the concentrations of acidic and basic centers are higher on K surface. Following the 1-min treatment, $-\Delta G_a^p$ is higher for acetone, *t*-BuOH, ethyl acetate, benzene and THF for KO 1. In the case of ZO 1, the same parameter is higher for *t*-BuOH and pyridine. The standard free energy of adsorption decreased in all other cases. However, $-\Delta H_a^p$ increased for all the tested probes adsorbed on KO 1 and ZO 1, except in the case of pyridine on ZO 1 – a significant decrease by ~70.0%. As concerns the effect of the plasma treatment time, changes in the thermodynamic magnitudes for the polar probes ($-\Delta G_a^p$ and $-\Delta H_a^p$) were small ($\leq$ 5.0 %) in the case of KO 4, but considerably larger (+45.0%) for ZO 4 except for the $-\Delta G_a^p$ values determined for nitromethane and acetonitrile, that underwent only moderate changes.

3.3. Surface topography analysis

Fig. 4 shows AFM micrographs (1000 × 1000 and 400 × 400 nm^2 areas) of K fiber, fresh (Fig. 4a and b) or treated with an oxygen plasma for 1 min (Fig. 4c and d) or 4 min (Fig. 4e and f).

The morphology of K sample consists of a surface of long nanofibrils with widths of about 10–20 nm. These nanofibrils are parallel to each other and also approximately parallel to the fiber axis (which runs from top to bottom for all the images presented in this work). This indicates a high degree of anisotropy and reflects the orientation of the rigid-rod PPTA macromolecules along the

Table 6
Specific free energies of adsorption of polar probes, $-\Delta G_a^p$(kJ mol^{-1}), calculated according to the method of Donnet et al.

T (K)	Polar probes	K	KO 1	KO 4	Z [24]	ZO 1	ZO 4
303	Benzene	4.0	4.8	5.0	6.6	4.0	4.4
	Nitromethane	13.8	13.5	13.8	12.9	11.2	11.6
	Acetonitrile	18.7	17.8	18.1	13.5	13.0	14.6
	Acetone	12.6	15.8	16.4			12.1
	t-Butyl alcohol	12.8			7.7	9.8	14.6
	Ethyl acetate	10.8	14.7	15.3	7.6	7.2	10.8
	Tetrahydrofuran	10.5	14.4	14.8	8.1	7.8	11.4
	Pyridine				12.8		
313	Benzene	4.1	5.2	4.7	6.8		3.8
	Nitromethane	13.5	13.7	13.1	12.8	10.8	10.7
	Acetonitrile	18.9	18.1	17.5	13.5	12.6	13.4
	Acetone	12.2	16.1	15.9			11.3
	t-Butyl alcohol	12.0	17.7	17.6	7.6	9.0	13.4
	Ethyl acetate	10.2	14.6	14.7	7.6	6.7	9.8
	Tetrahydrofuran	10.2	14.4	14.4	8.2		10.5
	Pyridine	17.9			12.7		
323	Benzene	4.0	4.4	4.4	6.7		
	Nitromethane	13.7	12.4	12.4	12.5	10.6	10.0
	Acetonitrile	18.5	16.5	16.6	13.2		12.5
	Acetone	11.3	14.6	15.2			10.3
	t-Butyl alcohol	11.3	15.9	16.7			
	Ethyl acetate	9.9	13.3	13.8	7.5		9.3
	Tetrahydrofuran	9.7	13.1	13.5	8.1		9.9
	Pyridine	17.7			12.5	24.1	
333	Benzene		4.4		6.6		
	Nitromethane	13.0	12.0	12.0	12.2		
	Acetonitrile	17.5	16.1	16.1	13.0		
	Acetone		14.0	14.5			
	t-Butyl alcohol		15.4	15.8	7.0	7.9	11.6
	Ethyl acetate	9.2	12.6	13.2	7.4		8.0
	Tetrahydrofuran		12.7	13.0	8.1		9.2
	Pyridine	17.0			12.3		
343	Benzene				7.0		
	Nitromethane	12.2	11.7	11.6	12.4		
	Acetonitrile	16.8	15.7	15.6	13.2		
	Acetone		13.6	14.0			
	t-Butyl alcohol		14.7	15.0	7.0	10.7	
	Ethyl acetate		12.2	12.6	7.5		
	Tetrahydrofuran		12.2	12.4	8.3		
	Pyridine	15.7			12.4	25.3	

Table 7
Specific (acid–base) contribution to the standard enthalpy of adsorption of several polar probes, $-\Delta H_a^p$(kJ mol^{-1}).

Polar probes	K	KO 1	KO 4	Z [24]	ZO 1	ZO 4
Benzene	3.7	10.3	13.5	5.0		
Nitromethane	24.5	29.5	30.9	17.8	20.7	34.6
Acetonitrile	34.0	37.0	37.7	17.1		47.0
Acetone	33.6	35.5	35.2			39.1
t-Butyl alcohol	39.4	47.4	44.7	13.9	28.4	43.3
Ethyl acetate		36.1	36.6	9.0		37.7
Tetrahydrofuran	22.6	33.7	33.9	7.6		33.2
Pyridine	39.5			16.4	4.9	

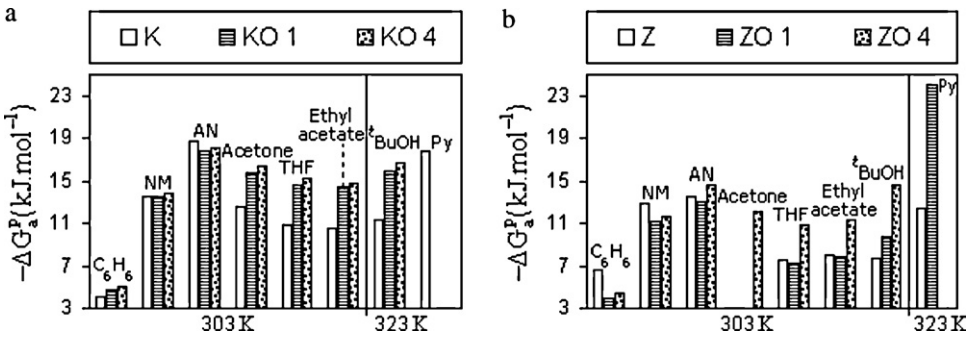

Fig. 3. $-\Delta G_a^p$ values calculated for the adsorption of different polar probes on the PPTA (a) and PBO (b) surfaces under study, at the specified temperature for each polar probe.

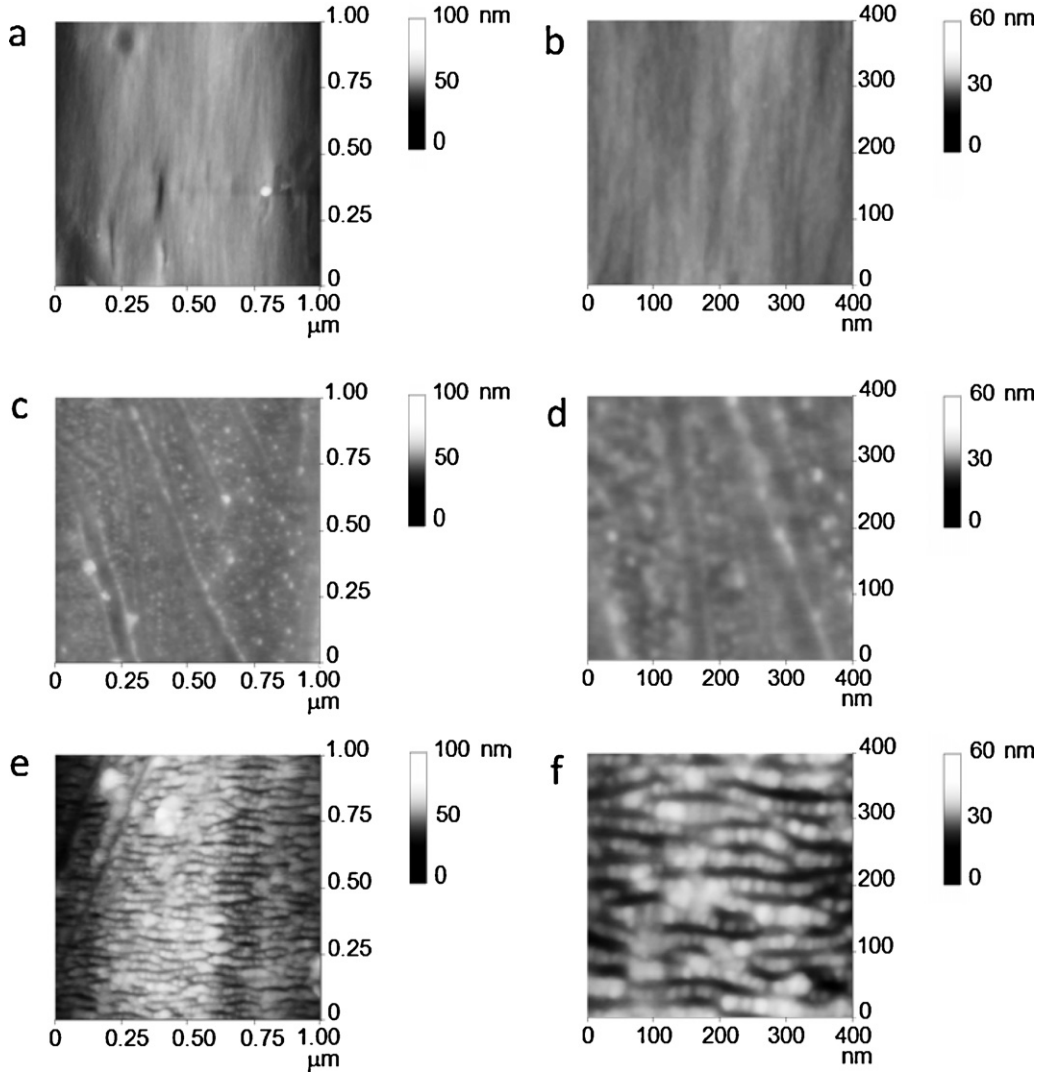

Fig. 4. AFM micrographs (1000 × 1000 and 400 × 400 nm^2 areas) of PPTA fibers, fresh (a and b) and treated with an oxygen plasma during 1 min (c and d) and 4 min (e and f).

direction of the fiber axis [25]. By contrast, this fibrillar morphology disappears from the surface of the samples treated with oxygen plasma even after the shortest time of exposure. In fact, samples treated for 1 min (Fig. 4c and d) show a predominantly dotted surface with some contribution of elongated features parallel to the fiber axis, thus retaining a certain degree of anisotropy. The longer treatment (4 min) leads to a completely different nanostructure to that of fresh PPTA, namely a rougher surface consisting of stripped globular features about 10–30 nm in width.

Fig. 5 shows AFM images of PBO, either untreated (Fig. 5a and b) or exposed to an oxygen plasma for 4 min (Fig. 5c and d). This material presents a morphology similar to that of PPTA, consisting of nanofibrils arranged parallel to the top-bottom direction along the fiber axis. The nanofibrillar structure can be best appreciated in Fig. 5b, which presents a more detailed height image. The nanofibrils were measured to be 15–20 nm wide, stretching parallel to the fiber axis over several tens of nm. Also in this sample some small patches/spots are apparent, which are interpreted to be contaminants [24]. It is worth mentioning that the small patches/spots observed on the Z surface have small lateral dimensions (up to several tens of nm,) and they have been detected in a small number [24]. The ZO 4 sample displays a different nanostructure to that of the Z fiber, possessing a much rougher surface with irregular features (elongated, approximately rounded, globular) together with a small contribution of features parallel to the fiber axis, thus retaining a certain degree of anisotropy (Fig. 5c and d).

4. Discussion

The values of q_d^0 and $(-\Delta S_a^0)$ increased in absolute value for PPTA after the 1-min oxygen plasma treatment (Table 4). This means that the affinity of the *n*-alkanes for KO 1 sample is greater than for K. The differential heat of adsorption of *n*-alkanes is related directly to the adsorption potential exerted by the microscopic structures, i.e., those to which the adsorbate molecules have access. According to this, the *n*-alkanes have easier access to the nonpolar part of the polymeric fiber (benzene rings) in KO 1 sample than in K sample. The increases in q_d^0 and $(-\Delta S_a^0)$ under plasma exposure were especially marked for *n*-octane and *n*-nonane. Such a trend may be related to changes in fiber surface microstructure (such as nanoroughness developed on the fiber surface during the plasma treatment) due to the non-polar character of these probes [25,50]. In this sense, it has been observed that, after the 1-min plasma treatment, the K surface losses a part of the anisotropy in the starting material and the degree of surface roughness increases (Fig. 4). From the point of view of chemical affinity, measured in terms of $-\Delta H_a^p$, it has been found that the interactions of all polar probes with KO 1 sample were stronger than on K surface

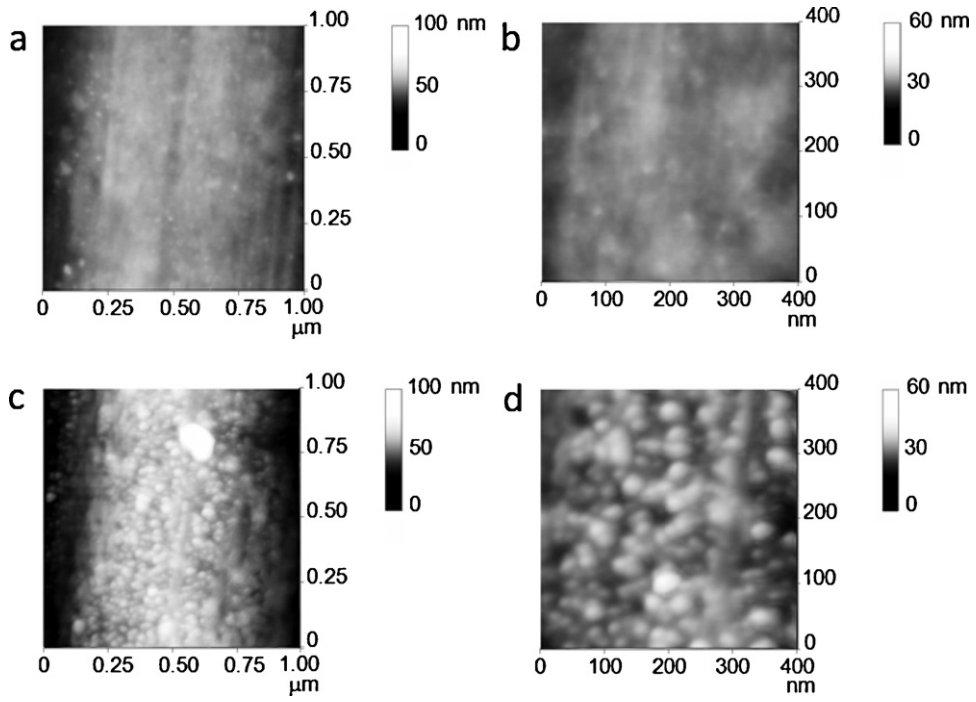

Fig. 5. AFM micrographs (1000 × 1000 and 400 × 400 nm^2 areas) of PBO fibers, fresh (a and b) and treated with oxygen plasma during 4 min (c and d).

(Table 7). However, in the cases of nitromethane and acetonitrile, the specific adsorption free energy ($-\Delta G_a^p$) did not increase under the plasma exposure. This indicates that the interactions of these two molecules with the adsorbent surface are favorable from an entropic point of view. It is probable that, due to the conformational changes underwent by the PPTA chains upon 1-min plasma treatment, the nitromethane and acetonitrile molecules do not have access to reactive sites (with acid–base or other properties) present at the KO 1 surface [25,51]. According to this series of findings, it is reasonable to believe that the 1-min oxygen plasma treatment leads to an increase in the amount of functional groups and, also, in the degree of surface roughness.

In the case of the longer treatment (4-min treatment), changes in the thermodynamic magnitudes upon interaction of *n*-alkanes (q_d^0, $-\Delta S_a^0$ and γ_D^s) and polar probes ($-\Delta G_a^p$ and $-\Delta H_a^p$) with KO 4, were small in all cases (<5.5%, see Tables 2, 4, 6 and 7) as compared with the KO 1 sample. However, KO 4 underwent significant changes in nanotopography. Thus, the 4-min treatment caused a severe loss in the degree of anisotropy with respect to K sample. The emergence of rounded domains with a typical width of 10–30 nm (Fig. 4) was observed. This could be justified on the basis of different extents of the chemical processes, i.e., reactions of oxidation and/or degradation of the material occurring at the polymer surface exposed to the plasma [52]. In general, the oxygen plasma can contribute to incorporate functional groups [22,46,53] and to remove material from the surface (etching) due to surface bombardment by active species in the plasma [22,54]. In the case of carbon fibers, it has been demonstrated that the surface concentration of oxygen (O/C ratio) increases as the oxygen microwave plasma conditions became increasingly severe (increase of exposure time and/or microwave power) until a maximum value was attained above which the O/C ratio remained constant [55,56]. Inagaki et al. [52] observed a similar behavior for a PPTA film that was modified by means of oxygen plasma. In this sense, it is expected that the O/C ratio will not increase even if the treatment conditions become more severe, what would mean that the kinetics of oxidation and degradation reactions are similar to each other.

Therefore, the IGC and AFM results lead one to believe that some elimination of polymeric material takes place as PPTA is exposed to oxygen plasma for 4 min. In this connection, the diameters of at least 50 PPTA fibers were measured using scanning electron microscopy (SEM). The mean value of KO 4 diameter decreased by about 1% with respect to K sample. This means that a slight elimination (or ablation) of polymeric material has taken place during the plasma treatment. On one hand, this justifies the small variations detected for the adsorption thermodynamic magnitudes since the atomic composition would slightly vary upon loss of polymeric material. On the other hand, there may be some radicalary recombination of certain segments of neighbor polymeric chains as a phenomenon associated with such loss. This behavior would justify, in part, the loss of anisotropy in the direction of the fiber axis observed for sample KO 4 [56].

In the case of PBO, the values of all adsorption thermodynamic magnitudes increased in absolute value following the 1-min treatment (see Tables 2, 4, 6 and 7), except the specific enthalpy ($-\Delta H_a^p$) for pyridine, which decreased considerably (by ~70.0%). However, the specific adsorption free energy ($-\Delta G_a^p$) for this molecule increased (by ~100.0%) with respect to Z sample (Table 6). According to Eq. (5), it can be deduced that the entropic term favors the interaction of pyridine with ZO 1. The melting process should be discarded for PBO fiber under the experimental conditions used in the plasma treatment. The maximum measured temperature during the plasma treatment was never higher than 80 °C. At such temperatures, the thermal stability of PBO fibers is still very high regardless any oxidative or inert atmosphere [24]. Therefore, one to conclude that the PBO surface has undergone some topographic changes following this plasma treatment. Indeed, it has been assumed previously that oxygen plasma is able to eliminate some material (physical etching); in fact, oxygen plasmas are used to remove organic contaminants from polymer surfaces [22].

Taking into account the fact that the commercial PBO surface is known to be heterogeneously covered with some contaminant substances [24] and that the values of q_d^0, $-\Delta S_a^0$ and γ_D^s have increased in absolute value following the 1-min treatment, it is reasonable to

believe that this treatment has removed at least part of these contaminants. This would justify the lower affinity ($-\Delta H_a^p$ value) of pyridine (DN = 33.10) for this surface. Indeed, the donor character of the surface would increase due to the high conjugation of the PBO polymeric chains (high π electron density along the chain). Moreover, thanks to the high rigidity of chemical bonds in the PBO chains (sp^2 bonds cannot rotate), pyridine would have easier access to the active sites at the polymer surface.

As concerns the 4-min treatment, the AFM images indicate that the contaminant that covered the starting PBO material has been removed (compare the micrographs for Z and ZO 4 samples in Fig. 5). Besides, the appearance of domains with irregular shapes (globular, elongated, etc.) all over the surface of sample ZO 4 was evident. On the basis of these results, and taking into account the fact that the values of the dispersive component of the surface tension of ZO 4 were larger than for ZO 1 (Table 4), it is reasonable to assume that cross-linking reactions between segments of neighbor polymeric chains have taken place.

Finally, taking into account that the surface of ZO 4, unlike that of KO 4, still maintains a certain degree of anisotropy along the fiber axis, it may be deduced that the PBO surface is comparatively more resistant to the 4-min oxygen plasma treatment than the PPTA one. In this sense, the diameter of at least 50 fibers was checked for samples Z and ZO 4 by SEM. It was observed that the mean value for ZO 4 sample (11.6 μm) was similar to that for Z (11.6 μm). Therefore, PBO is more resistant to the oxygen plasma treatment than PPTA. This could be expected from the higher degree of conjugation – and hence, lower chemical reactivity – of the former polymer.

According to these assertions, it is expected that the strength and/or the number of interactions that can establish the plasma-treated fibers to an organic resin such as an epoxy matrix may be substantially higher for the longer exposure (4 min) than the unmodified K and Z systems. The surface functionalization with polar groups and the nanoroughness developed with the longer exposure should favor the mechanisms involved in the adhesion phenomenon (chemical bonding and/or the mechanical interlocking). In regard to this, it was demonstrated that the interfacial adhesion between the PPTA or PBO fibers modified with an oxygen plasma treatment to an epoxy resin was improved regarding the untreated materials [11].

5. Conclusions

Changes in the surface properties of PPTA and PBO fibers exposed under equivalent conditions to an oxygen plasma have been comparatively investigated by means of IGC and AFM. There are clear size-exclusion behaviors, probably linked to the formation of nanopores or nanoroughness on the fiber surfaces under plasma exposure.

From adsorption of polar probes, IGC could only detect an increase in the number and strength of the acidic and basic sites present at the fiber surfaces. In any case, the 4-min treatment proved especially effective in favoring specific interactions on both modified surfaces, especially in the case of PBO.

The effects of oxygen plasma treatments of PPTA and PBO are similar to each other. Oxygen plasma exposure induces elimination reactions at the exposed surface, involving an increase in the degree of surface roughness, and a loss of polymeric material in the case of PPTA and a surface cleaning effect for PBO. In this regard, AFM measurements evidenced radical changes in the surface morphology at nanometer scale under the longer oxygen plasma treatment. The inherent anisotropy is replaced by cross-linked segments between neighboring polymeric chains, especially in the case of PPTA. SEM measurements demonstrated that the fiber diameter decreased in the case of PPTA, but did not change substantially for PBO. Therefore, under equivalent conditions, PBO is more resistant than PPTA to the oxygen microwave plasma.

For the PBO fibers, it has been observed that the outermost layer (contaminant substances) was removed with the plasma treatment. This indicates that the plasma has an important surface cleaning effect, considering that the usual surface cleaning treatments; i.e., by Soxhlet extraction, are much longer – even several days – than the plasma treatment used in this work (4 min).

Finally, it can be concluded that the longer exposure of oxygen plasma treatment can be able to improve the interfacial properties of composite systems reinforced with PPTA and PBO fibers without altering the bulk properties of the fibers. It was demonstrated that this longer exposure introduces polar groups onto both polymeric surfaces (PPTA and PBO). The IGC technique allows one to analyze the adsorption thermodynamic variables (especially the polar components) and estimate the chemical bonding associated to the adhesion phenomenon. On the other hand, it was proved that the modifications related to the surface nanoroughness degree also could improve the mechanical interlocking involved in an adhesion process as the dispersive components data of IGC and AFM topographic images have demonstrated.

Acknowledgements

The authors gratefully acknowledge the financial support from the European Union – project Growth G1RD-CT-2002-00747, from the 3rd PRI Asturias – project PB-EXP01-06 – and from the Spanish MEC – project CTQ2005-09105-C04-02. Special thanks are due to Toyobo (Japan) and DuPont de Nemours Int. (Switzerland) for supplying the PBO and PPTA samples, respectively.

References

[1] K. Tashiro, J. Yoshino, T. Kitagawa, H. Murase, K. Yabuki, Macromolecules 31 (1998) 5430.
[2] T. Kitagawa, H. Murase, K. Yabuki, J. Polym. Sci. B: Polym. Phys. 36 (1998) 39.
[3] C.L. So, R.J. Young, Composites A 32 (2001) 445.
[4] R.J. Davies, M.A. Montes-Morán, C. Riekel, R.J. Young, J. Mater. Sci. 36 (2001) 3079.
[5] M.A. Montes-Morán, R.J. Davies, C. Riekel, R.J. Young, Polymer 43 (2002) 5219.
[6] Y.K. Huang, P.H. Frings, E. Hennes, Composites B 33 (2002) 109.
[7] S.J. Bai, G.E. Price, Polymer 33 (1992) 2136.
[8] D.W. Tomlin, A.V. Fratini, M. Hunsaker, W.W. Adams, Polymer 41 (2000) 9003.
[9] K. Tamargo-Martínez, S. Villar-Rodil, J.I. Paredes, A. Martínez-Alonso, J.M.D. Tascón, Chem. Mater. 15 (2003) 4052.
[10] Toyobo Co Ltd. Technical Information, "PBO Fiber ZYLON". 2001.
[11] J.M. Park, D.S. Kim, S.R. Kim, J. Colloid Interface Sci. 264 (2003) 431.
[12] G.M. Wu, C.H. Hung, J.H. You, J. Polym. Res. 11 (2004) 31.
[13] G.M. Wu, Y.T. Shyng, Composites A 35 (2004) 1291.
[14] K. Luo, G. Li, J. Jin, S. Yang, J.J. Jiang, Macromol. Sci. B: Phys. 45 (2006) 631.
[15] J. Lange, E. Madre, K. Mai, R.J. Young, I. Ahmad, Composites A 32 (2001) 331.
[16] J.S. Park, M.K. Seo, T.J. Ma, D.R. Lee, J. Colloid Interface Sci. 252 (2002) 249.
[17] G.S. Sheu, S.S. Shyu, Compos. Sci. Technol. 52 (1994) 489.
[18] F. Severini, L. Formaro, M. Pegoraro, L. Posca, Carbon 40 (2000) 735.
[19] T. Ai, R. Wang, W. Zhou, Polym. Compos. 28 (2007) 412.
[20] B. Lindsay, M.L. Abel, J.F. Watts, Carbon 45 (2007) 2433.
[21] G.M. Wu, Mater. Chem. Phys. 85 (2004) 81.
[22] C.M. Chan, T.M. Ko, Surf. Sci. Rep. 24 (1996) 1.
[23] D.R. Lloyd, T.C. Ward, H.P. Schreiber, C.C. Pizaña (Eds.), ACS Symp. Ser., vol. 391, ACS, Washington, DC, 1989.
[24] K. Tamargo-Martínez, S. Villar-Rodil, J.I. Paredes, A. Martínez-Alonso, J.M.D. Tascón, M.A. Montes-Morán, Macromolecules 36 (2003) 8662.
[25] M.A. Montes-Morán, J.I. Paredes, A. Martínez-Alonso, J.M.D. Tascón, Macromolecules 35 (2002) 5085.
[26] J.R. Conder, C.L. Young, Physicochemical Measurement by Gas-chromatography, Wiley, New York, 1979.
[27] E.F. Meyer, J. Chem. Educ. 57 (1980) 120.
[28] S. Katz, D.G. Gray, J. Colloid Interface Sci. 82 (1981) 318.
[29] J.H. de Boer, The Dynamic Character of Adsorption, Clarendon Press, Oxford, 1953.
[30] F.L. Riddle, F.M. Fowkes, J. Am. Chem. Soc. 112 (1990) 3259.
[31] G.M. Dorris, D.G. Gray, J. Colloid Interface Sci. 77 (1980) 353.
[32] T. Hamieh, J. Schultz, J. Chromatogr. A 969 (2002) 17.
[33] T. Hamieh, J. Schultz, J. Chromatogr. A 969 (2002) 27.
[34] T. Hamieh, M.-B. Fadlallah, J. Schultz, J. Chromatogr. A 969 (2002) 37.
[35] T. Hamieh, J. Toufaily, A.H. Mouneimé, Chromatographia 73 (2011) 99.

[36] J.B. Donnet, S.J. Park, H. Balard, Chromatographia 31 (1991) 434.
[37] S. Rebouillat, J.B. Donnet, H. Guo, T.K. Wang, J. Appl. Polym. Sci. 67 (1998) 487.
[38] M.J. Partlett, P.S. Thomas, Polym. Int. 49 (2000) 495.
[39] M. Pérez-Mendoza, M. Domingo-García, F.J. López-Garzón, Langmuir 16 (2000) 7012.
[40] M.C. Almazán-Almazán, M. Pérez-Mendoza, I. Fernández-Morales, M. Domingo-García, F.J. López-Garzón, J. Chromatogr. A 1190 (2008) 271.
[41] M.C. Almazán-Almazán, J.I. Paredes, M. Pérez-Mendoza, M. Domingo-García, F.J. López-Garzón, A. Martínez-Alonso, J.M.D. Tascón, J. Colloid Interface Sci. 287 (2005) 57.
[42] H.H. Yang, Kevlar Aramid Fiber, Wiley, Chichester, 1993.
[43] T. Kitagawa, K. Tashiro, K. Yabuki, J. Polym. Sci. B: Polym. Phys. 40 (2002) 1281.
[44] V. Gutmann, The Donor–Acceptor Approach to Molecular Interactions, Plenum, New York, 1978.
[45] A. Van Asten, N. Van Veenedaal, S. Koster, J. Chromatogr. A 888 (2000) 175.
[46] G. Rezaei Behbehani, M. Hamedi, F. Hoseinpour Rajabi, Internet J Vib Spectrosc (2001), www.ijvs.com, 5, 6.
[47] M. Pyda, G. Guiochon, Langmuir 13 (1997) 1020.
[48] S. Rebouillat, J.C.M. Peng, J.B. Donnet, Polymer 40 (1999) 7341.
[49] C.A. Hunter, J.K.M. Sanders, J. Am. Chem. Soc. 112 (1990) 5525.
[50] M.C. Almazán-Almazán, J.I. Paredes, M. Pérez-Mendoza, I. Fernández-Morales, M. Domingo-García, F.J. López-Garzón, A. Martínez-Alonso, J.M.D. Tascón, J. Colloid Interface Sci. 293 (2006) 353.
[51] J.I. Paredes, S. Villar-Rodil, K. Tamargo-Martínez, A. Martínez-Alonso, J.M.D. Tascón, Langmuir 22 (2006) 4728.
[52] N. Inagaki, S. Tasaka, H. Hawai, J. Polym. Sci. A: Chem. 33 (1995) 2001.
[53] J.M. Grace, L.J. Gerenser, J. Dispersion Sci. Technol. 24 (2003) 305.
[54] J.R. Hollahan, A.T. Bell (Eds.), Techniques and Applications of Plasma Chemistry, Wiley, New York, 1974.
[55] J.P. Boudou, J.I. Paredes, A. Cuesta, A. Martínez-Alonso, J.M.D. Tascón, Carbon 41 (2003) 41.
[56] J.I. Paredes, A. Martínez-Alonso, J.M.D. Tascón, J. Colloid Interface Sci. 258 (2003) 276.